

Evidence for Bosonization in a three-dimensional gas of $SU(N)$ fermions

Bo Song,^{1,*} Yangjian Yan,^{2,*} Chengdong He,¹ Zejian Ren,¹ Qi Zhou,^{2,3,†} and Gyu-Boong Jo^{1,‡}

¹*Department of Physics, The Hong Kong University of Science and Technology,
Clear Water Bay, Kowloon, Hong Kong, China*

²*Department of Physics and Astronomy, Purdue University, West Lafayette, Indiana 47907, USA*

³*Purdue Quantum Science and Engineering Institute, Purdue University,
1205 W State St, West Lafayette, West Lafayette, IN 47907, USA*

(Dated: July 18, 2022)

A multi-component Fermi gas with $SU(N)$ symmetry is expected to behave like spinless bosons in the large N limit, where the large number of internal states weakens constraints from the Pauli exclusion principle [1]. Whereas blurring the boundary between bosons and fermions lies at the heart of multiple disciplines [2–5], bosonization of $SU(N)$ fermions has been experimentally tested only in a one-dimensional (1D) system so far [6]. Here, we report evidence for bosonization in a three-dimensional (3D) $SU(N)$ fermionic Ytterbium gas with tunable N . Using the column integrated momentum distribution, we measure contacts, the central quantity controlling dilute quantum gases [7–9], with a high signal-to-noise ratio in our system. We find that the contact per spin approaches a constant with a $1/N$ scaling in the low fugacity regime. This scaling signifies the vanishing role of the fermionic statistics in thermodynamics, and unfolds the intriguing nature of bosonization in 3D $SU(N)$ fermions. Our work suggests a new route of using contacts to explore multi-component quantum systems and their underlying symmetries.

Bosons and fermions exhibit intrinsically different properties because of the distinct underlying statistics. Strikingly, the boundary between bosons and fermions could become blurred under a variety of scenarios, ranging from the supersymmetry exchanging bosons and fermions to fermionization of strongly interacting bosons in 1D [2, 3]. In the latter case, hardcore bosons and noninteracting fermions share identical thermodynamical properties despite that their correlation functions are different. With increasing N in $SU(N)$ fermions, the Pauli exclusion principle becomes less effective in determining thermodynamical properties of a many-body system [1, 10]. Whereas this mechanism seems independent on the dimensionality of the system, bosonization of $SU(N)$ fermions have only be observed so far in 1D based on the measurement of the breathing mode [6].

In this work, we explore bosonization of a 3D $SU(N)$ fermion gas by measuring its central quantity, the so-called contacts, \mathcal{C} [7–9]. Through celebrated universal relations, contacts govern many other physical observables, such as the momentum distribution, the energy,

the pressure, and a variety of spectroscopies [7–9]. Therefore, the dependence of contacts on N directly provides us with the evidence of bosonization without resorting measuring other thermodynamical quantities. We choose ^{173}Yb atoms as our sample, in which the number of internal states accessible in experiments is highly tunable, ranging from one to six. Due to the strong decoupling between electronic and nuclear spins, interactions between nuclear spins are isotropic, providing the many-body system with a $SU(N)$ symmetry and consequently, a wide range of exotic phenomena [11–14].

Whereas the $SU(N)$ symmetry has been explored in optical lattices [6, 15–17], a spectroscopy [18], and collective excitations [6, 19], it is challenging to measure the rather small contact due to the weak interactions between ^{173}Yb atoms. To overcome this obstacle, we develop a new protocol to extract the contact from the column integrated momentum distribution without using the inverse-Abel transform, which allows a high signal-to-noise ratio (SNR). We observe that the contact increases as $(T/T_F)^{-3/2}$, when the temperature T/T_F decreases from $T/T_F=1.0$ to 0.55. When N is fixed, no change in the measured contact is observed for different spin constituents, confirming the isotropic interaction. We further change the number of nuclear spin component N and keep the number of atoms per component constant at the same temperature and trap geometry. We find a linear dependence of the contact with N . Consequently, the contact per spin approaches a constant with increasing N .

The observed scalings of contacts can be qualitatively understood as follows. As depicted in Fig. 1, in a balanced $SU(N)$ gas with N_0 atoms per spin state, a single atom with spin- σ interacts with $(N-1)N_0$ atoms in the other $(N-1)$ spin components with spin- σ' ($\sigma' \neq \sigma$) through the s -wave scattering. When interactions are spin-independent, each pair of atoms contributes an equal amount, c_{pair} , to the large momentum tail, $n_{3D}^{\sigma}(\vec{k}) = \mathcal{C}_0/k_{3D}^4$, where $\vec{k} = (k_x, k_y, k_z)$ is a 3D momentum vector and $k_{3D} = |\vec{k}|$ is much larger than k_F and other microscopic momentum scales. In the low fugacity regime where three-body correlations are negligible, $\mathcal{C}_0 = c_{\text{pair}}(N-1)N_0^2$, i.e., scaled with $(N-1)$ when the number of spin, N , is tuned. Correspondingly, if we consider the total momentum distribution,

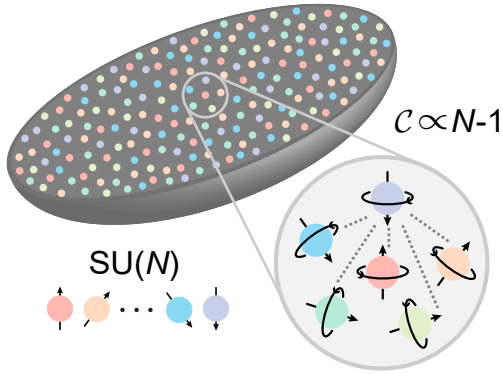


Figure 1: **Illustration of *s*-wave contacts in $SU(N)$ fermions with tunable spin.** Arrows with different colors and orientations denote the different nuclear spin states as large as $N=6$. Dashed lines represent pairs formed by two particles with different spins. Each pair contribute the same amount to the contact such that $\mathcal{C} \sim N - 1$.

$n_{3D}(\vec{k}) = \sum_{\sigma} n_{3D}^{\sigma}(\vec{k})$, we could define the total contact, $\mathcal{C}_{SU(N)} = NC_0 = c_{\text{pair}}N(N - 1)N_0^2$. Dividing $\mathcal{C}_{SU(N)}$ by N_t^2 , where $N_t = NN_0$ is the total particle number, we obtain that $\mathcal{C}_{SU(N)}/N_t^2 = c_{\text{pair}}(1 - 1/N)$.

In our experiment, *p*-wave scatterings are expected to be negligible, as the current temperature regime is smaller than the barrier of the *p*-wave interaction [20]. We, therefore, treat $SU(1)$ fermions as non-interacting systems. This is precisely the origin of the $1/N$ factor in the scaling of $\mathcal{C}_{SU(N)}/N_t^2$ with N . The Pauli exclusion principle suppresses the *s*-wave scattering between two atoms with the same spin, as well as their contributions to the *s*-wave contact. To have a comparison, we consider spinless bosons with the same N_t , T and the same scattering length, a_s . Though c_{pair} is independent on statistics, all $N_t(N_t - 1)/2$ pairs of particles in spinless bosons contribute to contacts such that the high momentum tail is written as $n_B(\vec{k}) = \mathcal{C}_B/k_{3D}^4$, where $\mathcal{C}_B = c_{\text{pair}}N_t(N_t - 1) \approx c_{\text{pair}}N_t^2$ for large N_0 , as the momentum distribution of identical particles doubles that of distinguishable particles. We obtain $\mathcal{C}_{SU(N)}/N_t^2 = \mathcal{C}_B/N_t^2(1 - 1/N)$, which shows that the *s*-wave contact of $SU(N)$ fermions approaches that of bosons with a $1/N$ scaling. Since $\mathcal{C}_0/N = (\mathcal{C}_{SU(N)}/N_t^2)N_0^2$, we use the contact per spin, \mathcal{C}_0/N , to capture this scaling with a fixed N_0 .

The experiment starts with degenerate fermions prepared in a crossed hybrid optical dipole trap (ODT) consisting of far-detuned 1064 nm and 532 nm laser light. A six-component Fermi gas of ^{173}Yb atoms, loaded from an inter-combination magneto-optical trap, is evaporatively cooled down to the temperature ~ 100 nK in the ODT in 6s. Along with the evaporation, an arbitrary spin mixture with $N=1,2,\dots,6$ is prepared by the use of optical pumping and blasting processes [21]. Next, we ex-

ponentially ramp up ODT to the final trap depth within 60 ms resulting in sufficiently large trap frequencies (see Methods for details). Finally, the momentum distribution after a 4ms time-of-flight expansion is recorded in the k_x - k_y plane by absorption imaging along the z direction using the resonant imaging light of $^1\text{S}_0 \rightarrow ^1\text{P}_1$ transition. In Fig. 2(b), a typical high-momentum tail is observed in the \mathcal{S} profile after the systematic noise is filtered out [22].

Our schematic protocol, for the high-precision measurement of the contact, is based on the momentum distribution of the atomic cloud after the time-of-flight expansion as shown in Fig. 2. Typically, to measure contacts from the momentum distribution, the atomic profile recorded in the 2D plane, which represents the column integrated momentum distribution, needs to be inverse-Abel transformed to 3D momentum distribution. However, inverse-Abel transform often intensifies measurement noise and exacerbates SNR because it involves a derivative of the atomic distribution, which inevitably limits our capability to detect contacts in a weakly interacting $SU(N)$ Fermi gas. To overcome this limitation, we extract contacts directly based on the weight of the high-momentum tail from a 2D time-of-flight image without using the inverse-Abel transform.

When k_{3D} is much larger than the inverse of the harmonic oscillator length and other microscopic momentum scales, $n_{3D}^{\sigma}(\vec{k})$ becomes isotropic in 3D and follows a scaling law, $n_{3D}^{\sigma}(k_{3D}) \rightarrow \mathcal{C}_0/k_{3D}^4$ where $n_{3D}^{\sigma}(k_{3D})$ is the atom number at k_{3D} . Here, we have used \mathcal{C}_0 to distinguish the original definition of contact from the scaled one, \mathcal{C} , used in our experiment. To be noted, in a spin-balanced Fermi gas with N components, atom density for each spin $n_{3D}^{\sigma}(k_{3D})$ is identical. Hereafter, it is normalized such that $\int n_{3D}^{\sigma}(k_{3D})d^3k_{3D} = 1$ in our experiment. Correspondingly, the column integrated momentum distribution, $n^{\sigma}(k) = \int_{-\infty}^{\infty} n_{3D}^{\sigma}(k_{3D})dk_z$, which follows $\int n^{\sigma}(k)2\pi kdk = 1$. The momentum is normalized by the Fermi wave number $k_F = \sqrt{2E_F m}/\hbar$ with the Fermi energy $E_F = \hbar\bar{\omega}(6N_0)^{1/3}$. Here $\bar{\omega}$ is the averaged trap frequency, m is the mass of ^{173}Yb and \hbar is the reduced Planck constant. Contact \mathcal{C} can be experimentally extracted from the high momentum plateau of a term $\mathcal{S} = 2/\pi \cdot k^3 n^{\sigma}(k)$ as follows (see Methods),

$$\mathcal{C} = \lim_{k \rightarrow \infty} \mathcal{S}(k) = \lim_{k \rightarrow \infty} \frac{2}{\pi} \cdot k^3 n^{\sigma}(k) = \frac{\mathcal{C}_0}{(2\pi)^3 N_0 k_F}. \quad (1)$$

Here, \mathcal{C} is naturally normalized by the atom number per spin N_0 and the Fermi wave number k_F . The key advantage of our protocol is that no transform gets involved resulting a high SNR ratio. To further diminish the noise of the atomic profile, we typically repeat the measurement ~ 100 times and obtain an averaged image as shown in Fig. 2(a), and then azimuthally average the momentum distribution profile with $\pm 0.2k_F$ moving average.

Because of the small scattering length of ^{173}Yb , contacts in our $SU(N)$ gas are contained in the large mo-

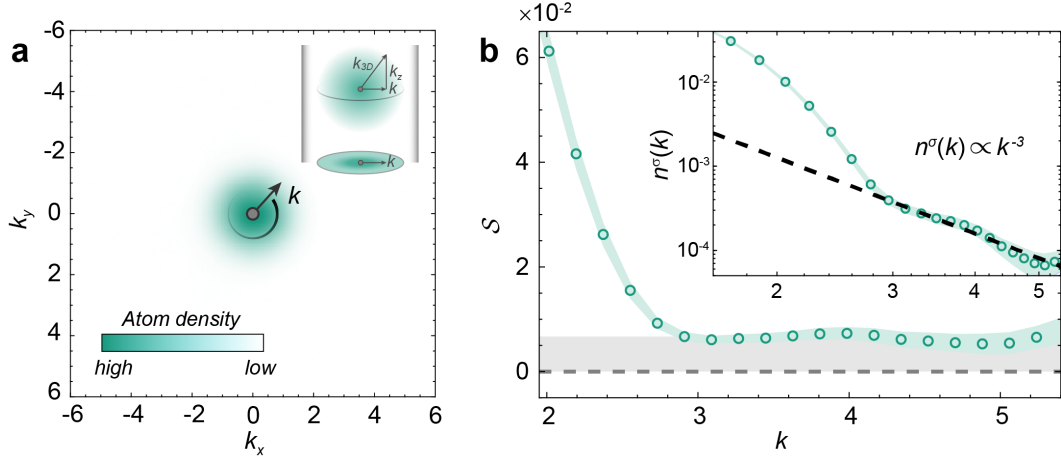


Figure 2: Measurement of the contact parameter from the momentum distribution. (a) Momentum distribution of ^{173}Yb atoms consisting $N = 6$ nuclear spin states after 4 ms time-of-flight expansion. Momentum here is normalized by the Fermi wave number k_F . Note that momentum profile outside $k \simeq 2.5$ has already been subtracted by the momentum profile of the spin-polarised gas ($N = 1$) with the same atom number. (b) $S = 2/\pi \cdot k^3 n^\sigma(k)$ is plotted as a function of momentum k in units of k_F . Inset is the momentum tail of azimuthally averaged atomic distribution $n^\sigma(k)$ in logarithmic scale with a dashed guideline of $n^\sigma(k) \propto k^{-3}$. The $n^\sigma(k)$ is normalized as $\int n^\sigma(k) 2\pi k dk = 1$. The finite value of the contact is determined from the plateau of the S profile in the range of $k = 3$ to 4. The green shaded area stands for the experimental uncertainty.

momentum tail with an extremely small amplitude that is below a thousandth of the maximum cloud density. To extract such high-momentum tail from the subtle density profile, we first filter out the systematic noise (e.g. interference fringes, imaging light fluctuation) using the statistical method. Our protocol is based on statistical image decomposition and projection methods using the data images as a basis set and compensating for unwanted fringes [22]. Secondly, we compare the high-momentum tail of $\text{SU}(N > 1)$ fermions with respect to non-interacting $\text{SU}(1)$ gases, and extract the high-momentum tail of $\text{SU}(N > 1)$ gases after subtracting the counterpart of $\text{SU}(1)$. This allows us to systematically eliminate the diffraction effect arising from atoms. Note that for a $\text{SU}(1)$ gas, we first separate the data set of $\text{SU}(1)$ into two parts and analyse them using a similar procedure.

In Fig. 3, we show the measured \mathcal{C} at temperatures between $T/T_F = 0.55$ and $T/T_F = 1$ for $\text{SU}(N=1,3,6)$. We change the number of components, $N=1,2,\dots,6$, but keep the same number of atoms per spin component $N_0=6.7 \times 10^3$ in a 3D harmonic trap with frequencies $(\omega_x, \omega_y, \omega_z) = 2\pi \times (1400, 750, 250)$ Hz and the averaged trap frequency $\bar{\omega} = (\omega_x \omega_y \omega_z)^{1/3} = 2\pi \times 640$ Hz. We post-select data images based on the atom number and temperature with tolerance of $\sim 0.1T_F$. As expected, a spin-polarized $\text{SU}(1)$ gas with negligible p -wave scatterings does not exhibit k^4 momentum tail within our experimental uncertainty while the finite contact is clearly observed for a $\text{SU}(6)$ or $\text{SU}(3)$ Fermi gas in Fig. 3(a). Within the temperature regime we explored, the contact increases as the temperature T/T_F decreases.

In Fig. 4, we test the scaling of the contact with the number of the spin components in $\text{SU}(N)$ Fermi gases. We first collapse data points in Fig. 3(a) to the Fermi temperature using $\mathcal{C} \propto (T/T_F)^{-3/2}$ shown in Fig. 3(b). The results clearly show that \mathcal{C} scales with $(T/T_F)^{-3/2}$. We further explore the dependence of the contact on N . Fig. 4(a) shows that \mathcal{C} depends linearly on $(N-1)$, and Fig. 4(b) demonstrates that $\mathcal{C}/N \sim \mathcal{C}_0/N$ approaches a constant with a $1/N$ scaling. All results are consistent with the qualitative picture we previously provided.

To measure $n^\sigma(k)$, we need to release atoms from the trap. Due to the absence of Feshbach resonance, interactions here cannot be turned off, unlike ^{40}K for studying s -wave contacts of two-component fermions [23]. Interactions lead to complex expansion dynamics that are difficult to compute in theory. Therefore, it is illuminating to theoretically study contacts of trapped gases before the expansion. We compute contacts in the temperature regime explored in the experiments, $0.55 \leq T/T_F \leq 1.0$, where the second order virial expansion works well and high order virial expansion are negligible [24, 25]. We evaluate the local contact at the position \vec{r} based on its local chemical potential $\mu_{loc} = \mu_0 - V(\vec{r})$, where μ_0 is the chemical potential at the center of the trap and $V(\vec{r})$ is the harmonic trapping potential. The total contact is obtained by integrating local contacts in the trap. The contact is written as $\mathcal{C}_0 = k_B T \frac{8\pi m}{\hbar^2} \left(\frac{k_B T}{\hbar \omega}\right)^3 z^2 \frac{a_s^2}{2^{3/2} \lambda} (N-1)$. $\lambda = \sqrt{2\pi \hbar^2 / (m k_B T)}$ is the thermal wavelength, and $z = e^{\beta \mu_{loc}}$ is the fugacity. In this temperature regime, the chemical potential μ_0 is well approximated by $\mu_0 =$

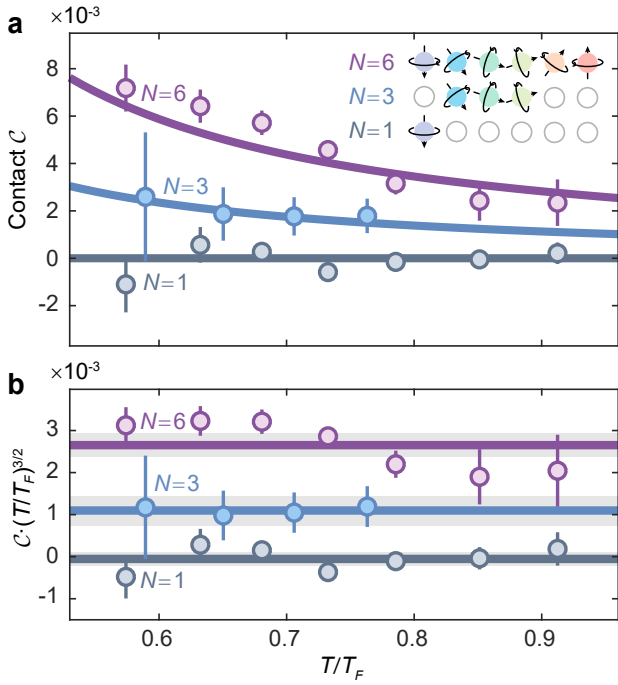


Figure 3: **Temperature scaling of contacts in $SU(N)$ fermions.** (a) Contacts are measured at different temperatures in the $SU(N)$ Fermi gases. The error bars represent one standard deviation in the plateau area of S profile. The solid curves are theoretical results multiplied by a factor of 6.5. Spin configuration of different $SU(N)$ gases are presented by arrows in spheres and the circle with empty inside indicates the absence of the spin state. Details of spin configurations and preparation of different $SU(N)$ gases are described in Methods. The result shows a good agreement with the temperature scaling $C \propto (T/T_F)^{-3/2}$. (b) Using the temperature scaling $C \propto (T/T_F)^{-3/2}$, contacts of $SU(N)$ gases at different temperatures are collapsed to the Fermi temperature $T = T_F$. The solid line are means of collapsed contacts. The shaded grey area indicates the experimental uncertainty which consists of the standard error and the standard deviation of each point.

$-T/T_F \cdot \log(6(T/T_F)^3)E_F$ [26]. We obtain

$$C = \frac{C_0}{(2\pi)^3 N_0 k_F} \approx \frac{ma_s^2}{6(2\pi)^{5/2} \hbar^2} \frac{E_F}{(T/T_F)^{3/2}} (N-1). \quad (2)$$

We observe that C scales with $N-1$ and $(T/T_F)^{-3/2}$ in the high temperature regime. Both scalings are consistent with the aforementioned experimental results, suggesting that interactions during the expansion do not change the scalings of the contact with T and N .

Using the virial expansion, the s -wave contact of spinless boson is also obtained explicitly in the same low fugacity regime (see Methods). We then find

$$C_{SU(N)} = N C_0 = \left(1 - \frac{1}{N}\right) C_B. \quad (3)$$

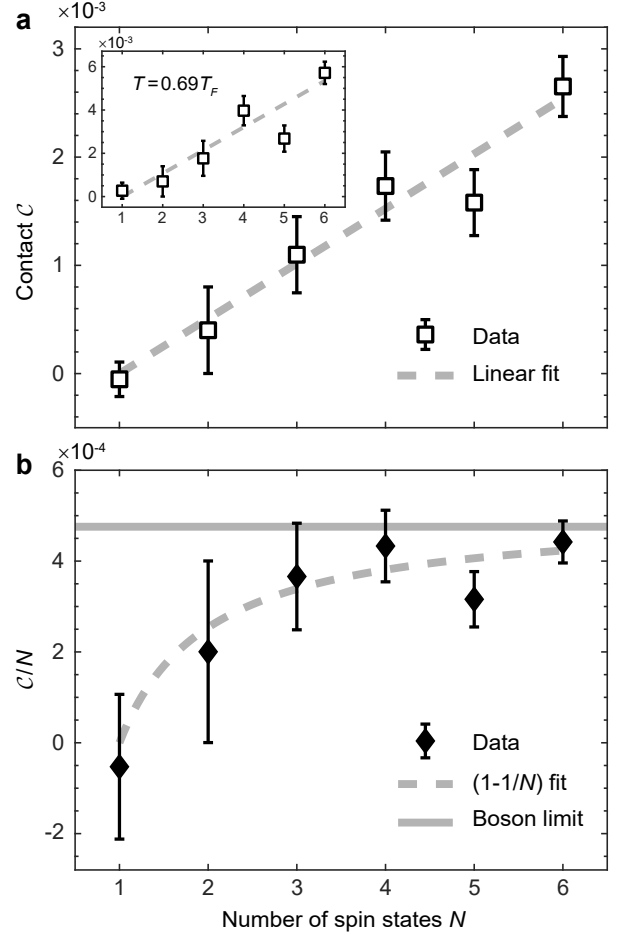


Figure 4: **Scaling of the contact in $SU(N)$ fermions with tunable spin.** (a) Contacts scale linearly with the number of spin components in a $SU(N)$ Fermi gas. Mean values of collapsed contacts at $T = T_F$ of $SU(N)$ gases are plotted as a function of number of spin states. The dashed line is a linear fit to $(N-1)$. Inset shows the contact at $T = 0.69 T_F$. (b) Contact per spin, C/N , as a function of N . The dashed line indicates a $(1-1/N)$ fit to the data. The horizontal solid line denotes the theoretical result of trapped bosons, $N_0 C_B / (8\pi^3 k_F N_t^2)$, multiplied by 6.5.

As contact is the central quantity to control the many-body system, Eq. (3) is a direct proof of the bosonization without resorting to any other quantities, such as the full momentum distribution.

Whereas scalings of the measured contacts with N and T after the expansion are consistent with theoretical results of trapped gases, experimental results lie systematically above theoretical ones, the former about 6.5 times larger than the latter (see Methods). It is interesting to note that such discrepancy was also observed in an experiment measuring contacts of a weakly interacting Bose-Einstein condensate of Helium-4 atoms [27]. Interactions remain finite during expansions in both cases. It is, therefore, possible that interaction effects during

the expansion lead to the aforementioned discrepancy. However, the current resolution limits our capability to measure the time dependence of contacts in the expansion, which by itself is an interesting question concerning the non-equilibrium dynamics of contacts. To avoid this issue and directly access contacts of trapped gases, an alternative scheme is the Bragg spectroscopy without the expansion [28].

We have focused on the low fugacity regime. With decreasing T , higher order virial expansions will become important. Though bosonization still exists, scalings with T and N are expected to change. It is desirable to study how the difference between contacts of $SU(N)$ fermions and spinless bosons scales with some powers of $1/N$. With further decreasing T down to below the superfluid transition temperature, our scheme of measuring contacts without using the inverse-Abel transform will provide us with an even richer playground to study contacts of superfluids with the $SU(N)$ symmetry. It is also generically applicable to other atomic systems including bosons.

^{*} These authors contributed equally to this work.
[†] Electronic address: zhou753@purdue.edu
[‡] Electronic address: gbjo@ust.hk

- [1] C. N. Yang and Y.-Z. You, *Chinese Physics Letters* **28**, 020503 (2011).
- [2] S. Weinberg, *The Quantum Theory of Fields* (University of Texas, Austin, 2000).
- [3] T. Giamarchi, *Quantum Physics in One Dimension* (Clarendon Press, Oxford, 2003).
- [4] Z. X. Li, A. Vaezi, C. B. Mendl and H. Yao, *Science Advances* **4**, eaau1463 (2018).
- [5] A. Cherman and D. Dorigoni, *Journal of High Energy Physics* **2012**, 173 (2012).
- [6] G. Pagano, M. Mancini, G. Cappellini, P. Lombardi, F. Schäfer, H. Hu, X.-J. Liu, J. Catani, C. Sias, M. Inguscio et al., *Nature Physics* **10**, 198 (2014).
- [7] S. Tan, *Annals of Physics* **323**, 2952 (2008).
- [8] S. Tan, *Annals of Physics* **323**, 2971 (2008).
- [9] S. Tan, *Annals of Physics* **323**, 2987 (2008).
- [10] X.-W. Guan, Z.-Q Ma and B. Wilson, *Physical Review A* **85**, 033633 (2012).
- [11] C. Wu, J.-p. Hu and S.-C. Zhang, *Physical Review Letters* **91**, 186402 (2003).
- [12] M. Hermele, V. Gurarie and A. Rey, *Physical Review Letters* **103**, 135301 (2009).
- [13] A. V. Gorshkov, M. Hermele, V. Gurarie, C. Xu, P. S. Julienne, J. Ye, P. Zoller, E. Demler, M. D. Lukin and A. M. Rey, *Nature Physics* **6**, 289 (2010).
- [14] M. A. Cazalilla and A. M. Rey, *Reports on Progress in Physics* **77**, 124401 (2014).
- [15] S. Taie, R. Yamazaki, S. Sugawa and Y. Takahashi, *Nature Physics* **8**, 825 (2012).
- [16] C. Hofrichter, L. Rieger, F. Scazza, M. Höfer, D. R. Fernandes, I. Bloch and S. Fölling, *Physical Review X* **6**, 021030 (2016).
- [17] H. Ozawa, S. Taie, Y. Takasu and Y. Takahashi, *Physical Review Letters* **121**, 225303 (2018).
- [18] X. Zhang, M. Bishop, S. L. Bromley, C. V. Kraus, M. S. Safronova, P. Zoller, A. M. Rey and J. Ye, *Science* **345**, 1467 (2014).
- [19] C. He, Z. Ren, B. Song, E. Zhao, J. Lee, Y.-C. Zhang, S. Zhang and G.-B. Jo, arXiv:1905.10815 (2019).
- [20] T. Fukuhara, Y. Takasu, M. Kumakura and Y. Takahashi, *Physical Review Letters* **98**, 030401 (2007).
- [21] B. Song, C. He, S. Zhang, E. Hajiyev, W. Huang, X.-J. Liu and G.-B. Jo, *Physical Review A* **94**, 061604 (2016).
- [22] In preparation (2019).
- [23] J. T. Stewart, J. P. Gaebler, T. E. Drake and D. S. Jin, *Physical Review Letters* **104**, 235301 (2010).
- [24] H. Hu, X.-J. Liu and P. D. Drummond, *New Journal of Physics* **13**, 035007 (2011).
- [25] M. Sun and X. Leyronas, *Physical Review A* **92**, 775 (2015).
- [26] D. Butts and D. Rokhsar, *Physical Review A* **55**, 4346 (1997).
- [27] R. Chang, Q. Bouton, H. Cayla, C. Qu, A. Aspect, C. I. Westbrook and D. Clément, *Physical Review Letters* **117**, 235303 (2016).
- [28] C. Carcy, S. Hoinka, M. G. Lingham, P. Dyke, C. C. N. Kuhn, H. Hu and C. Vale, *Physical Review Letters* **122**, 203401 (2019).
- [29] X.-J. Liu, *Physics Reports* **524**, 37 (2013).
- [30] S. E. Gharashi, K. Daily and D. Blume, *Physical Review A* **86**, 042702 (2012).
- [31] T. Busch, B. G. Englert, K. Rzazewski, and M. Wilkens, *Foundations of Physics* **28**, 549 (1998).
- [32] T.-L. Ho and E. J. Mueller, *Physical Review Letters* **92**, 160404 (2004).

Methods

Preparation of $SU(N)$ gases $SU(N)$ symmetric interaction in the ground state 1S_0 of ${}^{173}\text{Yb}$ atoms emerges from the decoupling between nuclear spin and orbital angular momentum ($J = 0$). Exploiting the energy splitting of the excited state in 3P_1 to our advantage, the narrow line-width transition ${}^1S_0(F = 5/2) \rightarrow {}^3P_1(F' = 7/2)$, with wavelength $\lambda = 556$ nm and natural line-width $\Gamma = 2\pi \times 181$ kHz, is used as a blasting light to remove unwanted m_F states of the ground manifold 1S_0 .

The preparation starts with a gas of spin-balanced six m_F states which is initially loaded in an optical dipole trap. A sequence of short pulses of σ^\pm optical blasting light resonance to transition $m_F \rightarrow m_F \pm 1$, is applied after the end of the evaporative cooling, where the temperature of atoms is $T \sim 100$ nK. The magnetic field of 13.6 G is applied leading to a Zeeman splitting of 8.4 MHz $\sim 46 \Gamma$ between two adjacent m_F states in the 3P_1 state. Take the preparation of a spin-balanced $SU(2)$ gas as an example, we shine pulses of resonant blasting light with transitions $m_F = 1/2 \rightarrow m'_F = 3/2$, $m_F = 3/2 \rightarrow m'_F = 5/2$ with σ^+ polarization to remove positive $m_F = 1/2$ and $m_F = 3/2$ respectively, and $m_F = -1/2 \rightarrow m'_F = -3/2$, $m_F = -3/2 \rightarrow m'_F = -5/2$ with σ^- polarization to remove negative $m_F = -1/2$ and $m_F = -3/2$ respectively, and the duration of each pulse is 5 ms. Following the similar method, arbitrary spin configuration of the $SU(N)$ ($N=1,2,\dots,6$) gas can be prepared by the combination of σ^+ and σ^- lights. The spin configurations of different $SU(N)$ gases used in the experiment are detected by optical Stern Gerlach effect [21] as shown in Fig. M1.

Notably, we use optical pumping to prepare spin polarized gases ($N = 1$) with different atom numbers. At the beginning of evaporation, we first optically pump most the atoms to the $m_F = 5/2$ state using another optical pumping light 400 MHz red detuned from the resonance with ${}^1S_0 \rightarrow {}^1P_1$ transition. The pumping pulse time is 300 ms. Note that we intentionally leave other spin states for the sake of the evaporative cooling. At the end of the evaporation, all the other remained spin states are removed by 556nm resonance light pulses similar to the procedure of $SU(N)$ gas preparation.

We further increase the trap depth to obtain large trap frequency, after the preparation of degenerate Fermi gases with different spin components at the temperature ~ 100 nK. $V(t)$, the trap depth of ODT is increased exponentially from the initial V_i to the final trap depth V_f in $t_f = 60$ ms with a time constant $\tau = 12$ ms as follows,

$$V(t) = ae^{t/\tau} + b \quad (4)$$

Where $a = (V_f - V_i)/(e^{t_f/\tau} - 1)$ and $b = V_i - a$. We have experimentally tested that T/T_F values of both non-interacting gases ($N = 1$) and weakly interacting gases

($N = 6$) are conserved during the ODT is ramped up as shown in Fig. M3.

Proof of the contact relation between \mathcal{C} and \mathcal{C}_0

Different from the original approach using the inverse Abel transform to get 3D normalized distribution $n_{3D}^\sigma(k)$ from 2D TOF image [23], the method in this letter is more robust against noise because the contact is directly extracted based on the radial averaged atomic distribution $n^\sigma(k)$ from 2D TOF image, illustrated in Fig. 2a. We calculate a term $\mathcal{S} = 2/\pi \cdot k^3 n^\sigma(k)$ as a function of momentum k . The value of contact is experimentally extracted from the end tail of \mathcal{S} profile. The contact \mathcal{C} is therefore defined as $\mathcal{C} = \lim_{k \rightarrow \infty} \mathcal{S}$, which is slightly different from the original definition \mathcal{C}_0 [7, 8], which stands for the contact. Contact defined here is naturally normalized by atom number per spin state N_0 and wave number k_F , and is associated with \mathcal{C}_0 as $\mathcal{C} = \mathcal{C}_0/((2\pi)^3 N_0 k_F)$. Here is the detail of the proof. In a spherical symmetry system which is confirmed experimentally, we start the derivation from the original definition of the contact \mathcal{C}_0 [7, 8],

$$\mathcal{C}_0 = (2\pi)^3 N_0 k_F \lim_{k_{3D} \rightarrow \infty} k_{3D}^4 n_{3D}^\sigma(k_{3D}) \quad (5)$$

Where 3D wave vector k_{3D} is normalized by k_F and 3D density $n_{3D}^\sigma(k_{3D})$ is normalized such that $\int n_{3D}^\sigma(k_{3D}) d^3 k_{3D} = 1$. The contact \mathcal{C} defined in this letter is written as,

$$\begin{aligned} \mathcal{C} &= \lim_{k \rightarrow \infty} \mathcal{S} \\ &= \lim_{k \rightarrow \infty} 2/\pi \cdot k^3 n^\sigma(k) \\ &= 2/\pi \lim_{k \rightarrow \infty} k^3 \int_{-\infty}^{\infty} n_{3D}^\sigma(k_{3D}) dk_z \end{aligned} \quad (6)$$

Here, we substitute the radial averaged atomic density with $n^\sigma(k) = \int_{-\infty}^{\infty} n_{3D}^\sigma(k_{3D}) dk_z$. From Eq. (5), for large k_{3D} , the 3D atomic density can be expressed as $n_{3D}^\sigma = \mathcal{C}_0/((2\pi)^3 N_0 k_F) \cdot k_{3D}^{-4} + \mathcal{O}(k_{3D}^{-5})$, in which $\mathcal{O}(k_{3D}^{-5})$ is the higher order term. Substitute n_{3D}^σ into Eq. (6), with wave vector relation $k_{3D}^2 = k^2 + k_z^2$,

$$\begin{aligned} \mathcal{C} &= \frac{2\mathcal{C}_0}{\pi(2\pi)^3 N_0 k_F} \lim_{k \rightarrow \infty} k^3 \int_{-\infty}^{\infty} \frac{dk_z}{(k^2 + k_z^2)^2} \\ &= \frac{\mathcal{C}_0}{(2\pi)^3 N_0 k_F} \end{aligned} \quad (7)$$

Theoretical model of contacts of $SU(N)$ fermions In the grand-canonical ensemble, the thermodynamic potential Ω for $SU(N)$ fermions can be Tayler-expanded in powers of small fugacity z (virial expansion),

$$\Omega = -k_B T Q(T) [Nz + Nb_2^{\text{ni}} z^2 + \frac{N(N-1)}{2} b_2(T, a_s) z^2 + \dots], \quad (8)$$

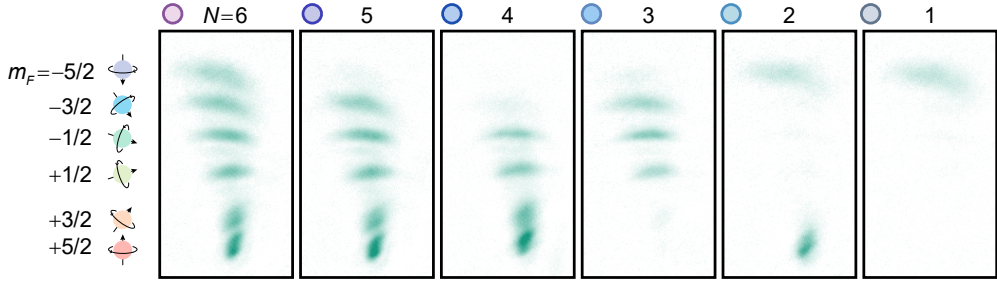


Figure M1: **Fermi gases with tunable spin components.** Unwanted spin components are removed by short pulses of resonant σ^+ and σ^- atomic transitions from $^1S_0 \rightarrow ^3P_1$ in an around 13.6 G magnetic field. From left to right, the number of spin is prepared from $N = 6$ to $N = 1$. Optical Stern-Gerlach detection is used to monitor the spin configurations and split sub-clouds from top to bottom are $m_F = -5/2$ to $m_F = 5/2$.

where $Q(T)$ is the single particle partition function, b_2^{ni} is the intraspecies second order virial coefficient which purely rise from particle statistics, and b_2 is the inter-species second order virial coefficient which typically depends on the scattering length and temperature. Using the adiabatic relation [8],

$$\left[\frac{\partial \Omega}{-a_s^{-1}} \right]_{T,\mu} = \frac{\hbar^2 N}{8\pi m} \mathcal{C}_0, \quad (9)$$

we obtain an virial expansion of the contact from Ref. [29],

$$\mathcal{C}_0 = k_B T \frac{4\pi m}{\hbar^2} Q(T) z^2 \frac{\partial b_2(T, a_s)}{\partial a_s^{-1}} (N - 1). \quad (10)$$

Comparing the Taylor expansion of the grand canonical potential Ω with the virial coefficient, we obtain

$$b_2(a_s, T) = Q_2/Q, \quad (11)$$

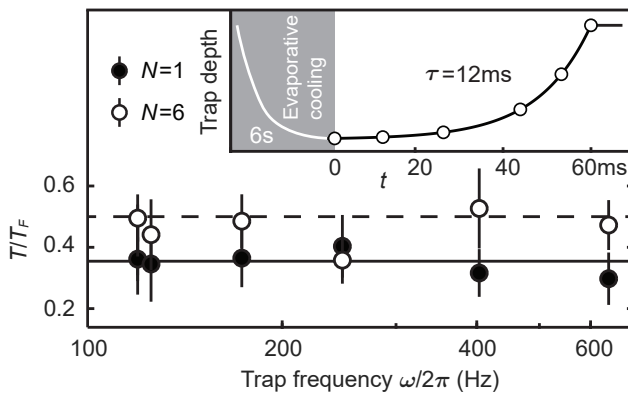


Figure M2: **The ramp-up of the optical dipole trap.** T/T_F of both non-interacting gases ($N = 1$) and weakly interacting gases ($N = 6$) are conserved during ramping up the optical dipole trap. The ODT is increased exponentially in $t_{\text{ramp}} = 60$ ms with the time constant $\tau = 12\text{ms}$ (inset). Gases with $N = 1$ and $N = 6$ components are initially prepared at $T = 0.35T_F$ and $0.5T_F$, respectively.

where Q_2 is the partition function of two particles of different species in the anisotropic trap. According to Ref. [30], one could transform the problem, to a very good approximation at high temperature, to a spherical harmonic trap with trapping frequency $\tilde{\omega}$ satisfies

$$3\tilde{\omega}^2 = \omega_x^2 + \omega_y^2 + \omega_z^2. \quad (12)$$

Using the energy spectrum of two particles under isotropic harmonic confinement at arbitrary scattering length obtained from solutions in Ref. [31] we can numerically determine the partition function as well as the derivative with respect to a_s^{-1} .

According to local density approximation, the virial coefficient for the trapped system can be related to that of the homogeneous system.

$$b_2 = b_2^{\text{homo}} / 2^{3/2}, \quad (13)$$

$$Q \approx (k_B T / \hbar \tilde{\omega})^3, \quad (14)$$

where $\tilde{\omega}^3 = \omega_x \omega_y \omega_z$. From Ref. [32], one obtain $b_2^{\text{homo}} = -2a_s/\lambda$, where λ is the thermal de Broglie length. Com-

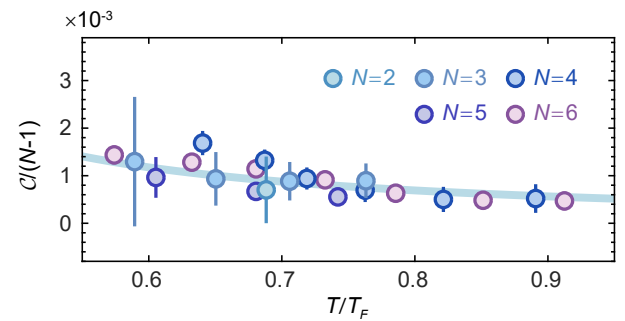


Figure M3: **Scaled contact vs temperature** Contact of different $SU(N)$ gases are scaled on the $N = 2$ components case by $\mathcal{C}/(N - 1)$. The solid curve is the theoretical simulation multiplied by a factor of 6.5.

bining the equations above, under LDA, we obtain

$$\mathcal{C}_0 = k_B T \frac{4\pi m}{\hbar^2} (k_B T / \hbar \bar{\omega})^3 z^2 \frac{2a_s^2}{2^{3/2} \lambda} (N - 1). \quad (15)$$

In the high temperature limit, $z = NN_0(\hbar \bar{\omega} / k_B T)^3$. The total contact of $SU(N)$ fermions is then written as

$$\mathcal{C}_{SU(N)} = N\mathcal{C}_0 = N_0^2 N (N - 1) \frac{2\sqrt{2}\pi m}{\hbar^2} \frac{(\hbar \bar{\omega})^3}{(k_B T)^2} \frac{a_s^2}{\lambda}. \quad (16)$$

Contact of single component Bose gas Applying the virial expansion to a single-component Bose gas, the thermodynamic potential Ω_B at high temperatures is written as

$$\Omega_B = -k_B T Q(T) [z + b_2^{\text{niB}} z^2 + b_2(T, a_s) z^2 + \dots]. \quad (17)$$

Here b_2 is the second order virial coefficient for two distinguishable particles, i.e., the same as that for the intraspecies b_2 for $SU(N)$ fermions, and b_2^{niB} is a term that accounts for bosonic statistics which is independent of the scattering length. Using the adiabatic relation [8],

$$\left[\frac{\partial \Omega_B}{-a_s^{-1}} \right]_{T,\mu} = \frac{\hbar^2}{8\pi m} \mathcal{C}_B, \quad (18)$$

we obtain an virial expansion of the contact,

$$\mathcal{C}_B = k_B T \frac{8\pi m}{\hbar^2} Q(T) z^2 \frac{\partial b_2(T, a_s)}{\partial a_s^{-1}}. \quad (19)$$

Using $z = NN_0(\hbar \bar{\omega} / k_B T)^3$, we obtain

$$\mathcal{C}_B = (N_0 N)^2 \frac{2\sqrt{2}\pi m}{\hbar^2} \frac{(\hbar \bar{\omega})^3}{(k_B T)^2} \frac{a_s^2}{\lambda}. \quad (20)$$

Compare \mathcal{C}_B and $\mathcal{C}_{SU(N)}$, we obtain

$$\mathcal{C}_{SU(N)} = \frac{N - 1}{N} \mathcal{C}_B. \quad (21)$$

In the limit $N \rightarrow \infty$, $\mathcal{C}_{SU(N)}$ approaches \mathcal{C}_B with a scaling of $1/N$.

Acknowledgement G.-B. J. acknowledges the generous support from the Hong Kong Research Grants Council and the Croucher Foundation through GRF16311516, and GRF16305317, GRF16304918, GRF16306119, C6005-17G and the Croucher Innovation grants respectively. Q. Z. is supported by NSF PHY 1806796.

Competing interests. The authors declare that they have no competing interests.

Data availability. The data that support the findings of this study are available from the corresponding authors upon reasonable request.